

Energy & Environmental Science

Accepted Manuscript



This is an *Accepted Manuscript*, which has been through the Royal Society of Chemistry peer review process and has been accepted for publication.

Accepted Manuscripts are published online shortly after acceptance, before technical editing, formatting and proof reading. Using this free service, authors can make their results available to the community, in citable form, before we publish the edited article. We will replace this *Accepted Manuscript* with the edited and formatted *Advance Article* as soon as it is available.

You can find more information about *Accepted Manuscripts* in the [Information for Authors](#).

Please note that technical editing may introduce minor changes to the text and/or graphics, which may alter content. The journal's standard [Terms & Conditions](#) and the [Ethical guidelines](#) still apply. In no event shall the Royal Society of Chemistry be held responsible for any errors or omissions in this *Accepted Manuscript* or any consequences arising from the use of any information it contains.

ARTICLE

Semi-Crystalline Photovoltaic Polymers with Efficiency Exceeding 9% in a ~300 nm Thick Conventional Single-Cell Device

Cite this: DOI: 10.1039/x0xx00000x

Received 00th January 2012,
Accepted 00th January 2012

DOI: 10.1039/x0xx00000x

www.rsc.org/T. L. Nguyen,^a H. Choi,^b S.-J. Ko,^b M. A. Uddin,^a B. Walker,^b S. Yum,^a J.-E. Jeong,^a M. H. Yun,^b T. J. Shin,^c S. Hwang,^a J. Y. Kim,^{*b} and H. Y. Woo^{*a}

We report a series of semi-crystalline, low band gap (LBG) polymers and demonstrate the fabrication of highly efficient polymer solar cells (PSCs) in a thick single-cell architecture. The devices achieve power conversion efficiency (PCE) of over 7% without any post treatment (annealing, solvent additive, etc.) and outstanding long-term thermal stability for 200 h at 130 °C. These excellent characteristics are closely related to the molecular structures where intra- and/or intermolecular noncovalent hydrogen bonds and dipole-dipole interactions assure strong interchain interactions without losing solution processability. The semi-crystalline polymers form a well-distributed nano-fibrillar networked morphology with PC₇₀BM with balanced hole and electron mobilities (h/e mobility ratio of 1~2) and tight interchain packing (π - π stacking distance of 3.57-3.59 Å) in the blend films. Furthermore, the device optimization with a processing additive and methanol treatment improves efficiencies up to 9.39% in a ~300 nm thick conventional single-cell device structure. The thick active layer in the PPDT2FBT:PC₇₀BM device attenuates incident light almost completely without damages in fill factor (0.71~0.73), showing a high short-circuit current density of 15.7~16.3 mA·cm⁻². Notably, PPDT2FBT showed negligible changes in the carrier mobility even at ~ 1 μ m film thickness.

Broader context

Polymer solar cells (PSCs) have great potential as a promising candidate for clean and renewable energy sources. PSCs are attracting increasing attention from both academia and industry, due to the demand for flexible, portable and solution processable low-cost photovoltaic devices to comply with increasing global energy demand. As results of many efforts for developing PSCs, the power conversion efficiency (PCE) of PSCs has been tremendously improved for the past decades. However, the low PCE is still a hurdle to overcome for commercial applications of PSCs. To further optimize PSCs, several challenges have to be considered including development of highly soluble and crystalline photovoltaic polymers to enable thick film production without damages in fill factor. In this work, we report a new series of semi-crystalline photovoltaic polymers, demonstrating a clear molecular design strategy, structure-property relationships and the highest PCE of 9.39% (reported so far) in a 290 nm thick single-cell device. We believe that our findings offer a bright future for the large scale commercialization of PSCs into daily-use electronic devices.

1. INTRODUCTION

Over the past few decades, polymer solar cells (PSCs) have made significant progress, showing their potential in low-cost, flexible, lightweight, portable and large-area energy-harvesting devices.¹ Considerable efforts have been dedicated toward the design of new materials, device architectures and processing techniques in order to improve the power conversion efficiency (PCE).²⁻⁵ Recently, bulk heterojunction (BHJ) PSCs, consisting

of low band gap (LBG) polymers (as an electron donor) mixed with C₆₀ or C₇₀ fullerene derivatives (as an electron acceptor), have shown promising performance with PCEs of 8~9% in single junction devices.⁶ Cao *et al.* reported highly efficient (9.2% PCE) inverted-type PSCs based on the benzodithiophene-thienothiophene copolymer (PTB7) with an amine-functionalized polymer interlayer as an indium tin oxide (ITO) surface modifier.⁷ With regard to a single cell having conventional geometry, Yu *et al.* further optimized PTB7 by

replacing thiophene with thienothiophene in the benzodithiophene moiety to yield a dithieno[2,3-d':3'-d'']benzo[1,2-b:4,5-b'']dithiophene-based polymer (PTDBD2) with a PCE of 7.6%.⁸ Chou *et al.* reported a new fluorinated quinoxaline-based copolymer (PBDT-TFQ) showing 8% PCE.⁹

To further improve PCEs, first and foremost, the molecular structure of LBG polymers should be carefully designed by considering its close relationship with the photovoltaic parameters, including short-circuit current density (J_{SC}), open-circuit voltage (V_{OC}) and fill factor (FF). Recently, highly efficient photovoltaic materials have been designed by introducing fluorine (F) atoms onto the polymeric chain.^{10,11} Fluorine has a small Van Der Waals radius (~1.35 Å) and is the most electronegative element with Pauling electronegativity of 4.0. The introduction of fluorine onto the periphery of an electron-deficient unit is a versatile strategy, because it not only minimizes any undesired steric hindrance along the polymer chains but also effectively stabilizes the highest occupied molecular orbital (HOMO) and lowest unoccupied molecular orbital (LUMO) levels. Furthermore, hole mobility improves upon fluorination, though a reverse trend has been observed in some cases.¹² The fluorine substituent often has great influence on inter- and intramolecular interactions,¹³⁻¹⁵ which play important roles in the solid-state polymer organization with a cofacial π - π stacking. An effective approach to planarize a polymer chain (without losing its solution processability) is to create a noncovalent attractive interaction between neighboring moieties *via* intramolecular hydrogen bonds and dipole-dipole interactions, *etc.* Noncovalent intramolecular O \cdots S interactions between alkoxy substituents and thiophene rings have been demonstrated to be effective for minimizing torsional angles within polymer backbones.¹⁶⁻¹⁸ On increasing the coplanarity of a polymer chain with close solid-state π - π stacking, both polaron and exciton delocalization and their transport characteristics can be improved.¹⁹⁻²¹

This study reports highly efficient new LBG polymer structures with a planar polymeric backbone formed *via* noncovalent intra- and interchain hydrogen bonds and dipole-dipole interactions, leading to highly ordered film morphologies, deep HOMO level, balanced electron and hole mobilities (hole/electron mobility ratio of 1~2) and exceptional device stability. Devices based on these polymers exhibit outstanding long-term thermal stability at 130 °C for over 200 h and the highest PCE over 9% in a conventional PSC having a single-cell device structure with a ~300 nm thick active layer.

2. RESULTS AND DISCUSSION

2.1. Molecular Design, Synthesis and Characterization.

The dialkoxyphenylene and benzothiadiazole (BT)-based monomers were prepared according to the procedures reported in the literature.²²⁻²⁴ 1,4-Dibromo-2,5-bis(2-hexyldecyloxy)benzene was reacted with three BT-based monomers, 4,7-bis(5-trimethylstannylthiophen-2-yl)-2,1,3-benzothiadiazole (M1), 4,7-bis(5-trimethylstannyl-thiophen-2-

yl)-5-fluoro-2,1,3-benzothiadiazole (M2) and 4,7-bis(5-trimethylstannylthiophen-2-yl)-5,6-difluoro-2,1,3-benzothiadiazole (M3) to yield poly[(2,5-bis(2-hexyldecyloxy)phenylene)-alt-(4,7-di(thiophen-2-yl)benzo[c][1,2,5]thiadiazole)] (PPDTBT), poly[(2,5-bis(2-hexyldecyloxy)phenylene)-alt-(5-fluoro-4,7-di(thiophen-2-yl)benzo[c][1,2,5]thiadiazole)] (PPDTFBT) and poly[(2,5-bis(2-hexyldecyloxy)phenylene)-alt-(5,6-difluoro-4,7-di(thiophen-2-yl)benzo[c][1,2,5]thiadiazole)] (PPDT2FBT), respectively, *via* Stille cross-coupling with Pd₂(dba)₃ as a catalyst in chlorobenzene using a microwave reactor (65~70% yield). The chemical structures and synthetic scheme for three polymers are shown in Fig. 1a and Scheme 1. The detailed synthetic procedures for the monomers are described in Supporting Information.^{22,23} The number-average molecular weight and molecular weight distribution were measured to be 17.8 (polydispersity index, PDI=2.4), 29.8 (2.4) and 42.6 kDa (2.8) for PPDTBT, PPDTFBT, PPDT2FBT, respectively (Table 1).

Three different types of dialkoxyphenylene and BT-based LBG copolymers were designed by carefully considering the planarity, chain curvature²⁵ and the resulting intermolecular orientations. The noncovalent attractive interactions between S (in thiophene) and O (in alkoxy groups), between S (in thiophene) and F, and between C-H (in thiophene) and N (in BT) minimize the torsional angle, thus maximizing the planarity of the polymer chain (Fig. 1b).^{13-18,26,27} Noncovalent coulomb interactions have been utilized to increase the planarity and ordering of polymer chains. Guo *et al.* demonstrated the use of noncovalent S \cdots O attractive interactions to fix the chain conformation with improved planarity in methoxy-substituted thiophene and bithiazoles (dihedral angle, ~0°) compared to unsubstituted (~22°) and methyl-substituted thiophene-containing analogues (~68°).¹⁷ S \cdots F interactions have been emphasized in controlling the stacking orientation in fluorinated benzobisbenzothiophenes by single-crystal X-ray analyses.¹³ Recently, Ratner and coworkers reported the role of nonbonding interactions in determining conformations of conjugated polymers and small molecules.²⁸ In this paper, the binding energy was calculated to be 2.2, 0.51 and 0.44 kcal/mol for CH \cdots N, O \cdots S and F \cdots S nonbonding interactions, respectively. The branched 2-hexyldecyloxy substituents endow great solubility in common organic solvents and PPDT2FBT were expected to be similar with that of PDTBT because of the small size of fluorine atoms and intrachain F \cdots S interactions. The introduction of alkoxy substituents on the phenylene ring was observed to decrease the torsional angle (18.4°–20.9°) *via* the S \cdots O noncovalent interaction compared to the alkyl-substituted structure (38.6°). Fig. S1† shows the minimum energy conformations of PPDTBT, PPDTFBT and PPDT2FBT. According to the torsional profiles for PPDT2FBT, there are two minimum energy conformations for the thiophene-dialkoxybenzene linkage. This means that the S \cdots O interaction is comparable with that of O \cdots H-C interaction (Fig. S1(b)†). The same argument can be applied to the thiophene-difluoro BT linkage

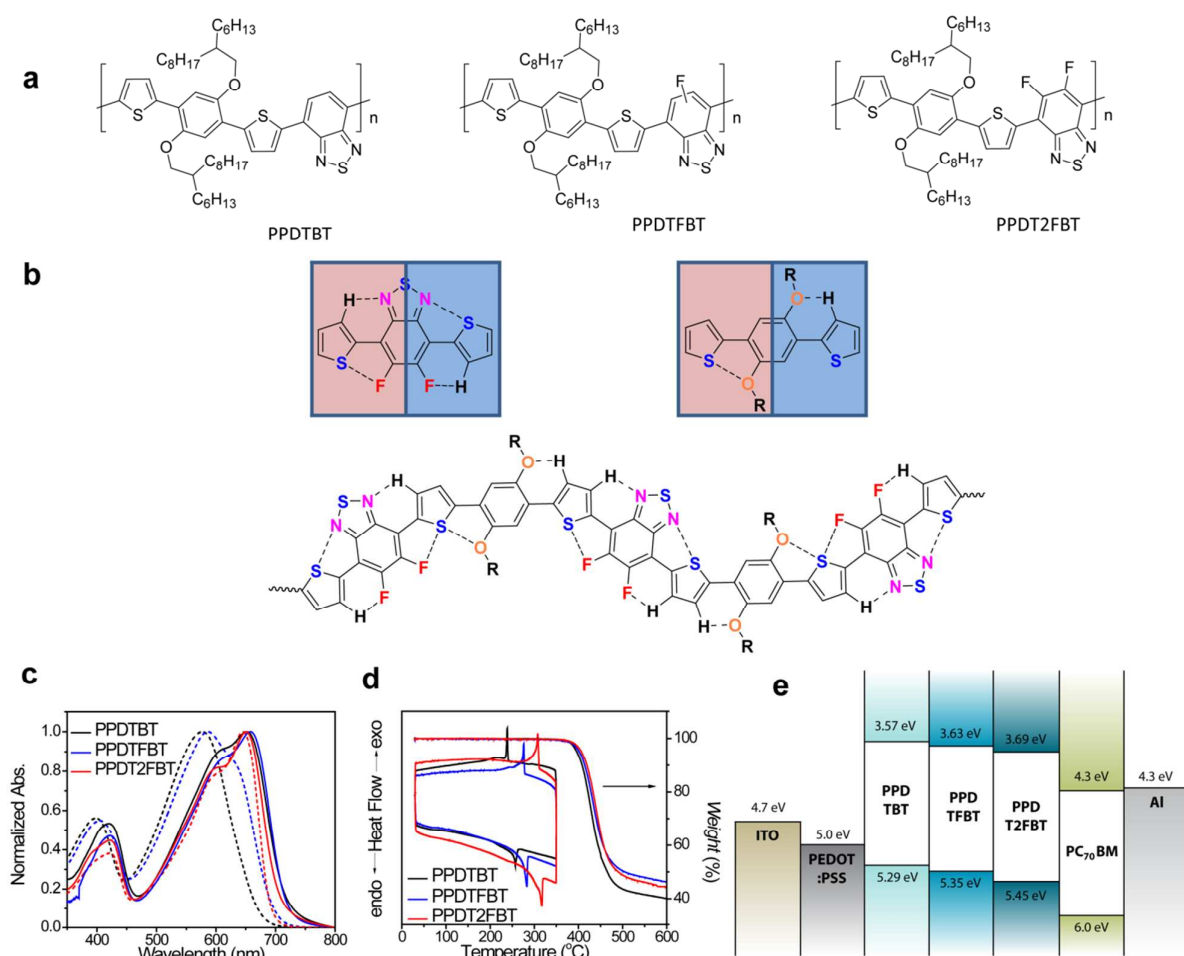


Fig. 1 (a) Chemical structures, (b) noncovalent attractive interactions within the polymer chain, (c) UV-vis absorption spectra (dashed: in chloroform, solid: in film), (d) TGA and DSC thermograms of PPDTBT, PPDTFBT and PPDT2FBT and (e) energy-band diagram.

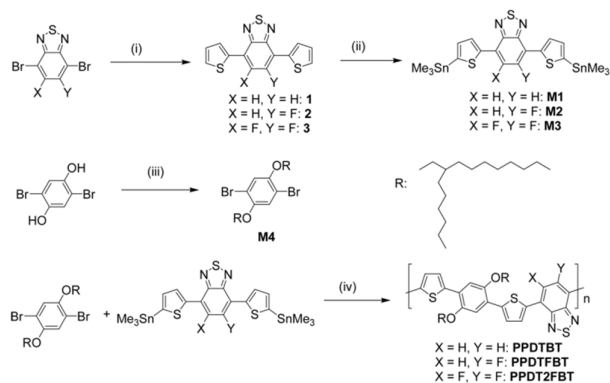
Table 1 Summary of photophysical-, electrochemical- and thermal properties of polymers.

Polymers	M_n [kDa] ^a	PDI	λ_{onset} (film) [nm]	E_g^{opt} [eV] ^b	HOMO [eV] ^c	LUMO [eV] ^d	T_d [°C] ^e	T_c [°C] ^f	T_m [°C] ^f
PPDTBT	17.8	2.4	720	1.72	-5.29	-3.57	396	239	257
PPDTFBT	29.8	2.4	720	1.72	-5.35	-3.63	397	276	283
PPDT2FBT	42.6	2.8	705	1.76	-5.45	-3.69	402	308	317

^aNumber-average molecular weight (M_n) determined by GPC with *o*-dichlorobenzene at 80 °C. ^bOptical band gap in film. ^cHOMO level was estimated from the tangential onset of oxidation ($E_{\text{ox}}^{\text{onset}}$) by cyclic voltammetry. HOMO (eV) = $-(E_{\text{ox}}^{\text{onset}} - E_{\text{ferrocene}}^{\text{onset}} + 4.8)$. ^dLUMO level was estimated from the HOMO value and optical band gap of the film. ^eDecomposition temperature (T_d) was determined by TGA (with 5% weight-loss). ^fCrystallization (T_c) and melting (T_m) temperatures were obtained from the peak maxima by DSC.

(Fig. S1(a)†). We guess that these minimum energy conformations are expected to repeat randomly in the polymeric backbone for the polymers, as displayed in Fig. 1b. In order to estimate interchain packing interactions, the binding energies were calculated by considering three types of cofacial interactions.³⁴ The head-to-tail (HT) configuration was found to be the most stable among the various possible configurations for all the polymers (Fig. S2†). The calculated binding energies of HT-type cofacial dimers were -18.7, -22.5, and -24.2 kcal·mol⁻¹ for PPDTBT, PPDTFBT and PPDT2FBT, respectively. In particular, the introduction of fluorine

substituents greatly affected the interchain packing by way of attractive C-F...H, F...S and C-F...π_F interactions in the adjacent polymeric chains.^{35,36} As shown in Fig. S2†, the replacement of methoxy substituents on the phenylene ring with ethyl groups destabilized the structure by ~3 kcal·mol⁻¹ because of the twisting in the main chain caused by the absence of S...O or O...H-C interactions. The HOMO levels were measured to be -5.29, -5.35 and -5.45 eV for PPDTBT, PPDTFBT and PPDT2FBT by cyclic voltammetry (CV) (Fig. S3†), respectively. The LUMO levels were estimated to be -3.57, -3.63 and -3.69 eV for PPDTBT, PPDTFBT and PPDT2FBT,

Scheme 1 Synthetic routes to the monomers and polymers^a

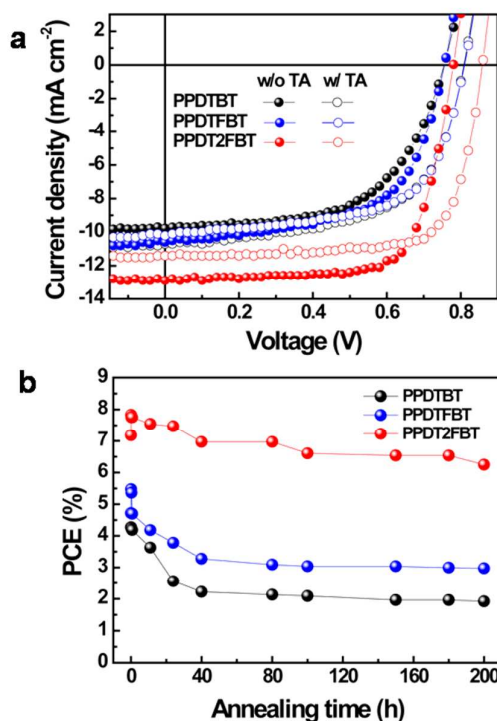
^aReagents and reaction conditions: (i) 2-tributylstannylthiophene, Pd₂(dba)₃, tris(*o*-tolyl)phosphine, toluene; (ii) (CH₃)₃SnCl, LiN(Pr-*i*)₂, THF; (iii) C₁₆H₃₃Br, KOH, 50% TBAB, toluene; (iv) Pd₂(dba)₃, tris(*o*-tolyl)phosphine, chlorobenzene.

respectively, from the HOMO values and the optical band gaps of the films. Though the HOMO and LUMO electronic structures were calculated to be similar for the three polymers (Fig. S4[†]), their energies were clearly stabilized upon fluorine substitution. The resulting energy band structures are also summarized in Fig. 1e.

Fig. 1c shows the normalized UV-vis absorption spectra of the polymers in chloroform and in the film. All the polymers exhibit broad absorption in the range of 350–750 nm with two distinct high and low energy bands attributed to the localized π - π^* and internal charge transfer transitions, respectively. In chloroform, the maximum absorption was measured at $\lambda_{\text{abs}} = \sim 575$ nm, ~ 585 nm and ~ 650 nm for PPDTBT, PPDTFBT and PPDT2FBT, respectively. More importantly, the shoulder peak at 650 nm was gradually enhanced with increasing fluorine substitution. In the film, three polymers show similar UV-vis profiles, where the spectra are red-shifted and the shoulder peak is substantially intensified, relative to those in solution. The differences in UV-vis spectra in the solution and film emphasize the facile interchain organization in the solid state. Optical band gaps were determined to be 1.72–1.76 eV for the polymer films. Thermal stability of the polymers was analyzed by thermogravimetric analysis (TGA) and differential scanning calorimetry (DSC) (Fig. 1d). PPDTBT, PPDTFBT and PPDT2FBT showed the decomposition onset temperatures with 5% weight loss at 396, 397 and 402 °C, respectively. Clear melting temperatures (T_m) at 257, 283 and 317 °C, and recrystallization points (T_c) at 239, 276 and 308 °C were measured for PPDTBT, PPDTFBT and PPDT2FBT, respectively, indicating clear crystalline nature of the polymers. This clearly indicates that the introduction of fluorine atoms has a significant effect on the thermal properties of the polymers. Detailed optical, electrochemical and thermal properties of the three polymers are summarized in Table 1.

2.2. Photovoltaic Device Characterization.

We investigated the photovoltaic properties of the polymers with a simple device architecture of ITO/PEDOT:PSS/polymer:PC₇₀BM/Al (PEDOT: PSS, poly(3,4-ethylenedioxythiophene): polystyrene sulfonic acid; PC₇₀BM, [6,6]-phenyl-C₇₁ butyric acid methylester). To



optimize the donor and acceptor (D:A) blend ratio, polymer:PC₇₀BM blend films were processed using *o*-dichloro-**Fig. 2** (a) Current density versus voltage (*J*-*V*) characteristics (w/o TA: without thermal annealing, w/ TA: with thermal annealing) and (b) temporal stability (at an annealing temperature of 130 °C) of polymer:PC₇₀BM PSCs. All devices were prepared from *o*-dichlorobenzene solutions.

Table 2 Device characteristics of polymer:PC₇₀BM-based PSCs with thermal annealing (solvent: DCB, blend ratio: 1:1.5).

Polymer	Thermal annealing ^a	J_{SC} (mA/cm ²)	V_{OC} (V)	FF	PCE (%) Best / Ave
PPDTBT	No	9.77	0.76	0.58	4.27 / 4.12
	Yes	10.40	0.81	0.61	5.08 / 4.89
PPDTFBT	No	10.6	0.76	0.59	4.72 / 4.38
	Yes	10.2	0.81	0.62	5.11 / 5.02
PPDT2FBT	No	12.9	0.78	0.71	7.18 / 6.94
	Yes	11.40	0.86	0.74	7.26 / 7.06

^aThermal annealing at 130 °C for 10 min.

benzene (DCB) as a solvent (Fig. S5[†] and Table S1[†]). For all polymers, devices with a D:A weight ratio of 1:1.5 showed the best performance (PCE: 4.27%, 4.72% and 7.18% for PPDTBT, PPDTFBT and PPDT2FBT, respectively). The device using PPDT2FBT exhibited the highest PCE of 7.18% with a J_{SC} of 12.9 mA·cm⁻², V_{OC} of 0.78 V and FF of 0.71. This shows one of the highest PCE values reported so far for conventional PSCs without any post-treatments (*i.e.*, thermal, solvent annealing and additives, *etc.*). Upon thermal annealing (130 °C for 10 min), V_{OC} and FF were substantially improved for the three polymer systems (Fig. 2a, Table 2). The V_{OC} increased from 0.76–0.78 V to 0.81–0.86 V and the FF improved by ~0.03. This must be due to morphological changes in the photoactive layer and improved contact between the active layer and electrode. Similar results have been reported.³⁷ Temporal stabilities of the devices were also characterized by annealing at 130 °C for 200 h under nitrogen (Fig. 2b). After

thermal annealing for 200 h, the PPDTBT device showed ~55% decrease in PCE. Interestingly, the PSCs based on PPDTFBT and PPDT2FBT showed a substantial improvement in temporal stability, showing 37% and 13% reductions in PCE, respectively. This remarkable device stability must be closely related to the stronger intermolecular interaction and higher interchain ordering, which is also consistent with the TGA and DSC measurements. Furthermore, relatively small morphological changes were detected for the PPDT2FBT:PC₇₀BM blend film after thermal annealing, compared to those of other two polymers and P3HT blends by atomic force microscopy (AFM) (Fig. 3). Until now, there have been few reports on conjugated polymers achieving both high efficiency of over 7% and long-term thermal stability of over 200 h in PSCs (Table S2†, S2-1†).

Processing additives offer an efficient way to control the morphology of the active layer by selectively solvating one of the components in BHJ systems.³⁸⁻⁴⁰ Several additives were tested to modulate the morphology of the blended films prepared from a 1 wt% chlorobenzene (CB) solution, where the clearer additive effects were observed compared to the films from DCB solutions. In contrast to poor performances of the devices fabricated without processing additives (Fig. S6† and Table S3†), devices with additives showed substantial improvements in photovoltaic properties. Among the tested

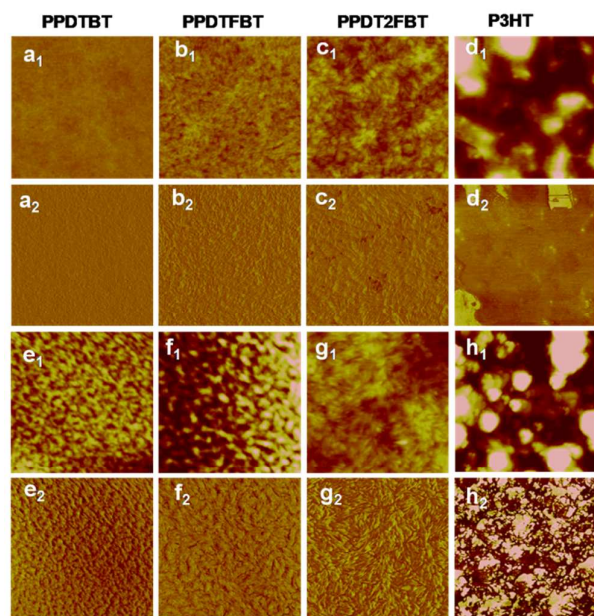


Fig. 3 Tapping-mode AFM topography and phase images of polymer:PC₇₀BM blend films (solvent: DCB) before and after thermal treatment at 130 °C for 200 h. Before thermal treatment: PPDTBT (a₁, a₂), PPDTFBT (b₁, b₂), PPDT2FBT (c₁, c₂), P3HT (d₁, d₂). After thermal treatment: PPDTBT (e₁, e₂), PPDTFBT (f₁, f₂), PPDT2FBT (g₁, g₂), P3HT (h₁, h₂). The size of all images is 1.5 μm × 1.5 μm.

additives, diphenyl ether (DPE) was found to be an appropriate processing additive for our polymers. The addition of DPE to CB (CB:DPE = 98:2 by volume) led to remarkable enhancements in device performances for the three polymeric structures, showing ca. 5–8% PCE values (Fig. 4). PPDTBT:PC₇₀BM and PPDTFBT:PC₇₀BM devices showed the best PCE with a film thickness of ~170 nm. Interestingly, the PPDT2FBT blend film exhibited the best efficiency using a thick (290 nm) film (as shown in Fig. S7† and Table S4†). Fig.

4a and Fig. 4b show the *J-V* characteristics and external quantum efficiency (EQE) of the devices with DPE. Table 3 summarizes the detailed photovoltaic parameters. The PPDT2FBT device showed the highest PCE of 8.64% with a J_{SC} of 15.73 mA·cm⁻², V_{OC} of 0.78 V and FF of 0.71, reaching EQE values of over 80% in the range of 470–550 nm with a maximum EQE of 82.5% at 490 nm (Fig. 4b). These enhancements in J_{SC} and FF by the addition of DPE are closely related to the strong interchain ordering with the recovery of the strong shoulder peak (originating from strong intermolecular packing and/or π - π stacking) of polymer:PC₇₀BM blend films in UV-vis spectra (Fig. 5). In addition, we also measured a remarkable temporal stability of PPDTFBT- and PPDT2FBT-blended films (in CB without DPE) at 130 °C for 200 h, compared to PPDTBT and P3HT based devices (Fig. S8a†). For devices with the processing additive (DPE), poor thermal stability was measured, showing a gradual decrease of PCE, compared to the devices without DPE (Fig. S8b†). It has been recognized previously that thermal treatment induces agglomeration with concomitant decrease in device performance with processing additives. The solvent additive allows the components to remain partially dissolved, affecting the morphology and diffusion rate of fullerene molecules in the polymer matrix, promoting the growth of fullerene agglomerates. This can accelerate phase separation between the polymer and fullerene moieties during heat treatment, adversely affecting device performance.⁴¹

To further optimize the PPDT2FBT device, the top of the active layer was treated with methanol (MeOH). Solvent treatments can be an effective strategy for simultaneously enhancing all device parameters.^{42,43} Fig. 4c and Fig. 4d show *J-V* characteristics of optimized, MeOH treated, PPDT2FBT:PC₇₀BM devices as measured in our laboratory and certified by the Korea Institute of Energy Research (KIER), respectively. More than 50 devices were fabricated for device optimization. The best performing device exhibited a PCE of 9.39% (average PCE = 9.21%) with J_{SC} of 16.30 mA·cm⁻², V_{OC} of 0.79 V and FF of 0.73 (Table 3). The EQE values of these devices are above 80% in the range of 460–570 nm with a maximum EQE of 83.6% at 490 nm (inset of Fig. 4c). The surface morphologies of PPDT2FBT:PC₇₀BM films with and without MeOH treatments were characterized by AFM (Fig. S9†). There were no observable changes in the AFM images, indicating that the effects of MeOH treatment do not arise from reconstruction of the film surface. Similar data and the detailed studies on the MeOH treatment effects have been reported previously. Bazan and Heeger *et al.* reported that MeOH treatment enhanced photovoltaic efficiency by increasing the internal electric field and surface potential by Kelvin probe force microscopy (KPFM) and impedance measurements. Additionally, the series resistance decreased and the shunt resistance increased after methanol treatment, in good agreement with the observed improvements in J_{SC} and FF.^{42,43} A certified PCE of 8.78% was obtained by KIER (Fig. 4d and Fig. S10†) from a UV-epoxy encapsulated sample. This PCE was ~5% lower than the average PCE as measured in our laboratory, which could be attributed to non-ideal encapsulation.^{7,44} The certified results confirm that the measured PCE values of over 9%, as obtained in our laboratory, are reasonable. Furthermore, this work is the first report that showcases efficiency over 9% with a conventional-type, 290

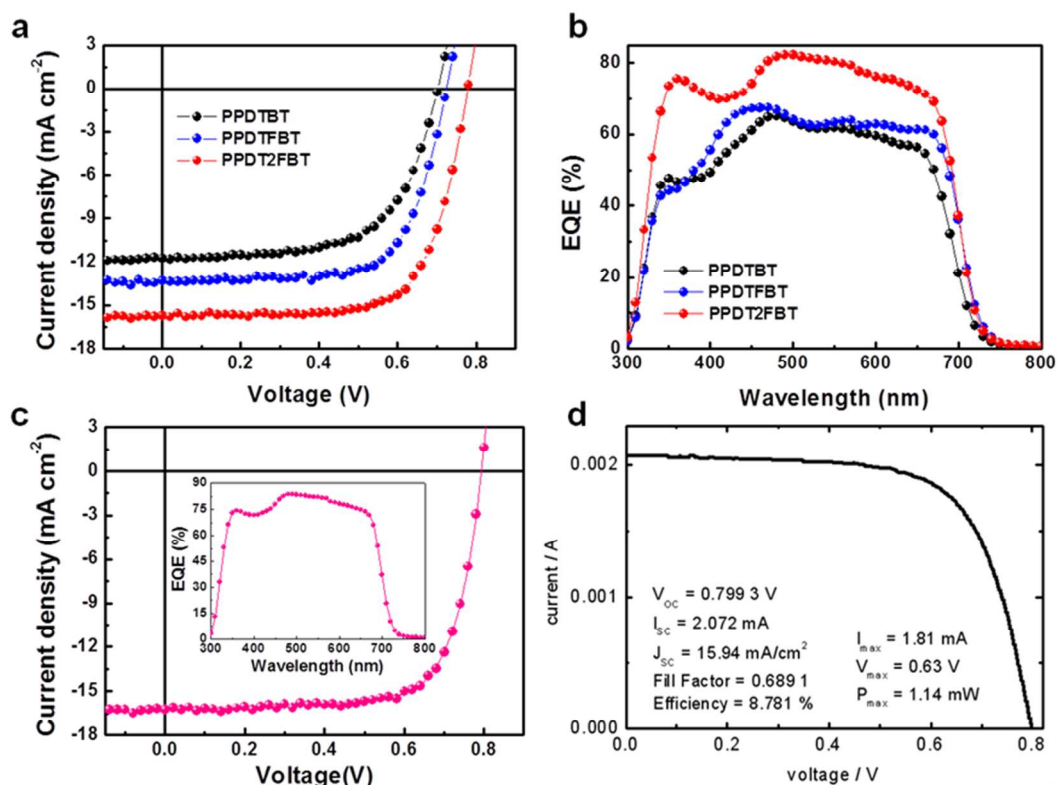


Fig. 4 Photovoltaic characteristics of polymer:PC₇₀BM-based devices fabricated using a CB:DPE solvent mixture. (a) Current density versus voltage (*J-V*) characteristics and (b) external quantum efficiency (EQE) of polymer:PC₇₀BM-based PSCs. (c) *J-V* characteristics of the optimized PPDT2FBT:PC₇₀BM-based PSC obtained from our laboratory and (d) certified by the KIER, respectively (c, d: with MeOH treatment). The inset of fig. 4c shows the EQE values over 80% in a range of 460-570 nm with the maximum EQE of 83.6% at 490 nm.

Table 3 Summary of photovoltaic characteristics (prepared from a solvent mixture of CB and DPE).

Polymer	Active layer thickness (nm)	MeOH treatment	J_{SC} (mA cm ⁻²)	V_{OC} (V)	FF	J_{SC} [Cal.] ^a (mA·cm ⁻²)	PCE (%)	
							Best	Ave
PPDTBT	170		11.73	0.70	0.63	11.77	5.17	5.04
PPDTFBT	175	No	13.29	0.73	0.69	12.88	6.64	6.45
PPDT2FBT	290		15.73	0.78	0.71	15.59	8.64	8.39
PPDT2FBT	290	Yes	16.30	0.79	0.73	15.94	9.39	9.21

^a J_{SC} [cal.], calculated J_{SC} from a EQE curve.

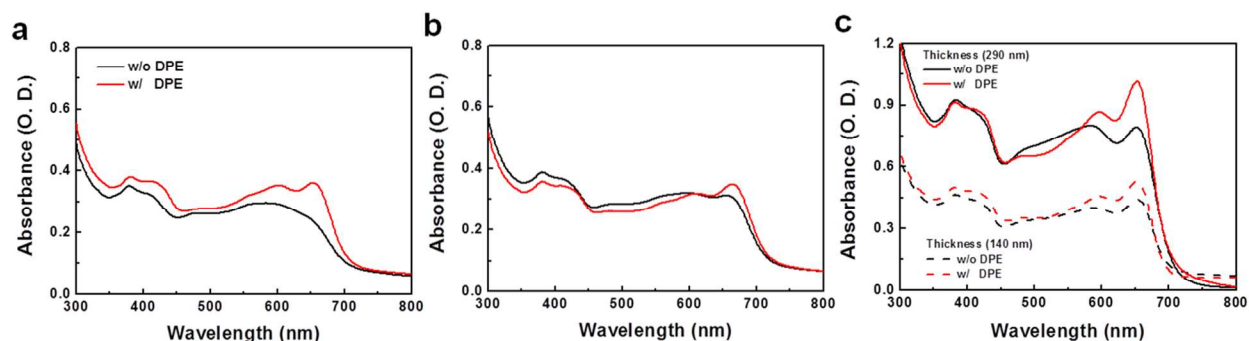


Fig. 5 UV-vis absorption spectra of polymer:PC₇₀BM blend films based on (a)PPDTBT, (b)PPDTFBT and (c)PPDT2FBT. The films were prepared with CB (w/o DPE) and mixed CB:DPE (98:2 vol.%, w/ DPE) as a solvent.

nm thick, single cell structure without any additional interfacial layer (Table S5†). The high PCE and device thickness also suggest a meaningful approach for real commercial applications of PSCs. Although remarkable improvements in PCE have been reported in PSCs, the device thickness is on the order of ~100 nm. It is of great importance to develop photovoltaic materials which can function effectively at the greater film thickness. It is not currently viable to fabricate uniform and defect-free films on the order of 100 nm thickness using industrial solution casting techniques. Most previous PSCs showed the performance degrades with concomitant decrease in FF, with increasing film thickness. This must be closely related to space charge accumulation and charge recombination losses which become stronger with thicker films. It is noteworthy to emphasize that ~300 nm thick active layer in the PPDT2FBT:PC₇₀BM device attenuates incident light almost completely without damages in fill factor (0.71~0.73), showing a high J_{SC} of 15.7~16.3 mA·cm⁻². These superior properties are closely related to the molecular structures and pronounced crystalline morphology in film.

2.3. Morphological and Charge Transport Characteristics.

The nanoscale morphology of polymer:PC₇₀BM blend films (in CB) was studied by high-resolution transmission electron microscopy (HR-TEM) and tapping mode AFM. In Fig. 6, TEM images show large domains with diameters of 100–300 nm for the PPDTFBT and PPDT2FBT blend films fabricated without DPE, whereas the PPDTBT films show featureless morphologies. Macrophase separation in the PPDTFBT and PPDT2FBT blend films limits the probability for exciton dissociation by reducing donor/acceptor interfacial areas, leading to poor J_{SC} and FF values by charge recombination loss.^{9,45} In contrast, the blend films with DPE show a clear morphological change for all polymers, forming well-distributed nano-fibrillar structures where a bicontinuous interpenetrating network may be formed in BHJ films with PC₇₀BM. These fibrillar structures are expected to enhance the charge-carrier mobility, J_{SC} , FF and the resulting photovoltaic performance of PSCs.^{44,46} Surface topography and phase images of the three blend films obtained from AFM measurements are consistent with morphologies observed in HR-TEM images (Fig. 7).

In order to quantify charge carrier mobilities, hole-only (ITO/PEDOT:PSS/polymer:PC₇₀BM/Au) and electron-only (FTO/polymer:PC₇₀BM/Al, FTO: fluorine-doped tin oxide) diodes were prepared⁴⁷ using optimized BHJ films (CB:DPE = 98:2 vol%) with various film thickness (200 ~ 1000 nm) and their J - V characteristics were analyzed by the space charge limited current (SCLC, J_{SCL}) method. The potential loss due to the series resistance of the ITO and the built-in potential were carefully considered in order to ensure accuracy in the measurements. The J - V characteristics show a quadratic dependence on voltage over a range of several volts and inverse cubic dependence on the film thickness, consistent with the Mott-Gurney relationship (equation 1),^{48,49}

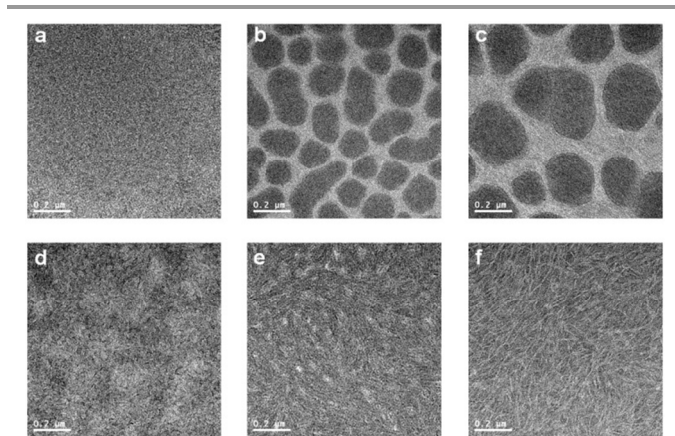


Fig. 6 HR-TEM images of polymer:PC₇₀BM films without (a~c) and with DPE (d~f). PPDTBT (a, d), PPDTFBT (b, e) and PPDT2FBT (c, f).

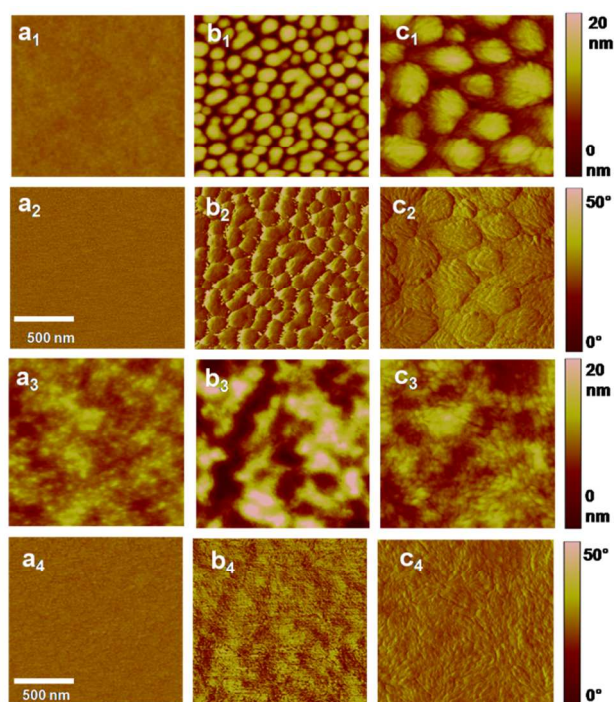


Fig. 7 Tapping-mode AFM topography (a₁~c₁, a₃~c₃) and phase (a₂~c₂, a₄~c₄) images of polymer:PC₇₀BM blend films. Without DPE: PPDTBT (a₁, a₂), PPDTFBT (b₁, b₂) and PPDT2FBT (c₁, c₂). With DPE: PPDTBT (a₃, a₄), PPDTFBT (b₃, b₄) and PPDT2FBT (c₃, c₄). The size of all images is 1.5 μm x 1.5 μm.

$$J_{SCL} = 9 \epsilon_0 \epsilon_r \mu V^2 / (8L^3) \quad (1)$$

where ϵ_0 is the free-space permittivity, ϵ_r is the dielectric constant of semiconductor, μ is the mobility, V is the applied voltage and L is the thickness of active layer.

The average hole and electron mobilities were determined to be $\mu(\text{hole}) = 3.2 \times 10^{-4}$, 5.5×10^{-4} and 3.0×10^{-3} cm²/Vs, and $\mu(\text{electron}) = 2.8 \times 10^{-4}$, 4.2×10^{-4} and 1.5×10^{-3} cm²/Vs for PPDTBT, PPDTFBT and PPDT2FBT devices, respectively. Plots of films with similar thickness can be found in Fig. 8, while additional plots with films of various thickness can be

found in Fig. S11† and Table S6†. All the polymers showed well balanced hole/electron mobility ratios in the range of 1~2 with various film thicknesses. PPDT2FBT showed ~1 order

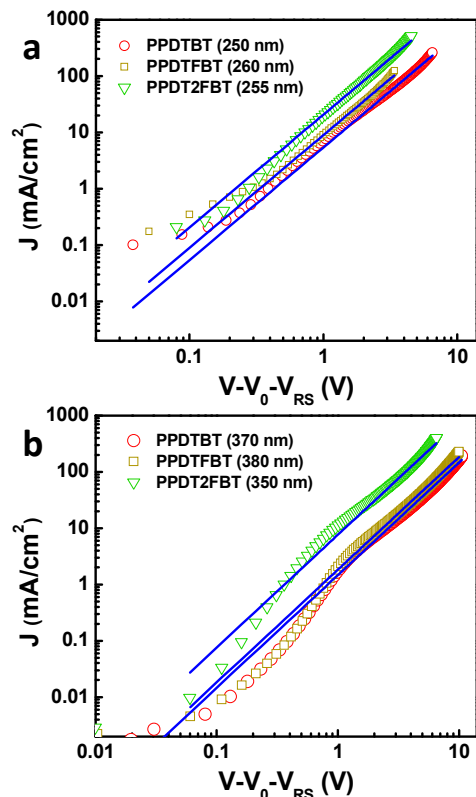


Fig. 8 *J-V* characteristics of (a) hole- and (b) electron-only devices based on polymer:PC₇₀BM blend films (solvent: CB:DPE = 98:2 vol%). Blue lines represent fits of the curves using the Mott-Gurney relationship.

higher hole and electron mobilities relative to other two polymers. Notably, PPDT2FBT showed negligible changes in the carrier mobility even at ~1 μm film thickness. These SCLC results are consistent with the PCE data of PPDT2FBT, showing no decrease in V_{OC} and FF with 290 nm thick active layer, resulting in a high J_{SC} of 15.7~16.3 mA·cm⁻² due to the increased light absorption.

To further understand the detailed film morphology of the three polymers with/without PC₇₀BM and before/after additive treatments, the molecular arrangements and packing characteristics of the thin films were studied by grazing incidence wide angle X-ray scattering (GIWAXS).^{43,50} Fig. 9 shows GIWAXS patterns for pristine polymer and polymer:PC₇₀BM blend films prepared from CB solutions with and without DPE. From the GIWAXS profiles, packing parameters were extracted and are listed in Table S7. Pronounced reflection peaks of (100), (200), and (300) in the out-of-plane direction were observed in the pristine PPDTBT film, showing a lamellar spacing of 18.9 Å (Fig. 9a and Fig. S12†). For the pristine PPDTFBT and PPDT2FBT films, the lamellar spacing calculated from the (100) diffraction peak was slightly increased to 20.7 Å. On increasing the number of

fluorine substituents on the BT unit, the in-plane lamellar diffraction peak was also intensified (strongest in PPDT2FBT). Therefore, the presence of fluorine atom may induce a face-on lamellar orientation coexisting with the edge-on lamellar stacks, which may facilitate effective three-dimensional charge transport. The PPDTBT sample showed no π - π stacking (010) peak in the out-of-plane direction. Interestingly, the (010) peak ($d \sim 3.7$ Å) in the out-of-plane direction becomes pronounced by the introduction of fluorine substituents. The π - π stacking distance was shorter in PPDT2FBT (3.72 Å) than in PPDTFBT (3.78 Å), which indicates stronger cofacial interchain orientation between the neighboring chains. Upon addition of DPE to the pristine polymer films, similar trends were observed with increased scattering intensity, indicating more pronounced interchain orientation with DPE. The GIWAXS patterns of polymer:PC₇₀BM blend films are shown in Fig. 9c and 9d. The lamellar spacing for polymer:PC₇₀BM blend samples was measured to be 19.1–19.9 Å for the three structures, showing similar spacings in the pristine polymer films. Upon addition of DPE, the diffraction patterns are clearer without noticeable changes in the lamellar spacing. We also observed further reduction in the π - π stacking distance (3.57–3.59 Å) for the PPDTFBT:PC₇₀BM and PPDT2FBT:PC₇₀BM films with DPE, indicating an intensified interchain orientation upon addition of DPE. Interestingly, the blend films with DPE show shorter π - π stacking distances than those of the pristine polymers (PPDTFBT: 3.78 Å and PPDT2FBT: 3.72 Å). The solvent additive allows the components to remain partially dissolved and affects the morphology and diffusive rate of PC₇₀BM in the polymer matrix. This may allow a longer time for polymer chains to self-organize into highly ordered intermolecular structures.⁵¹

3. CONCLUSION

In summary, a series of dialkoxyphenylene-BT containing semi-crystalline LBG polymers were synthesized with noncovalent conformational locking to enhance chain planarity, intermolecular ordering and thermal stability without the loss of solution processability. The polymers formed well-distributed interpenetrating nano-fibrillar networked morphologies with PC₇₀BM, showing well-balanced hole and electron mobilities. Notably, PSCs based on these polymers exhibited PCEs of up to 9.39% in a 290 nm thick conventional single-cell device structure without any additional interfacial layer. The thick active layer (290 nm) in the PPDT2FBT:PC₇₀BM device enabled strong light absorption, yielding a high J_{SC} of 15.7~16.3 mA·cm⁻² without the loss in V_{OC} and FF. It is of great importance to develop photovoltaic materials which can function effectively at the thicker film which can absorb solar light completely and is viable to be produced using industrial solution processing techniques. These remarkable device characteristics with the great thickness are closely related to the highly ordered organization of polymer chains *via* noncovalent attractive interactions, showing nano-fibrillar structures in TEM

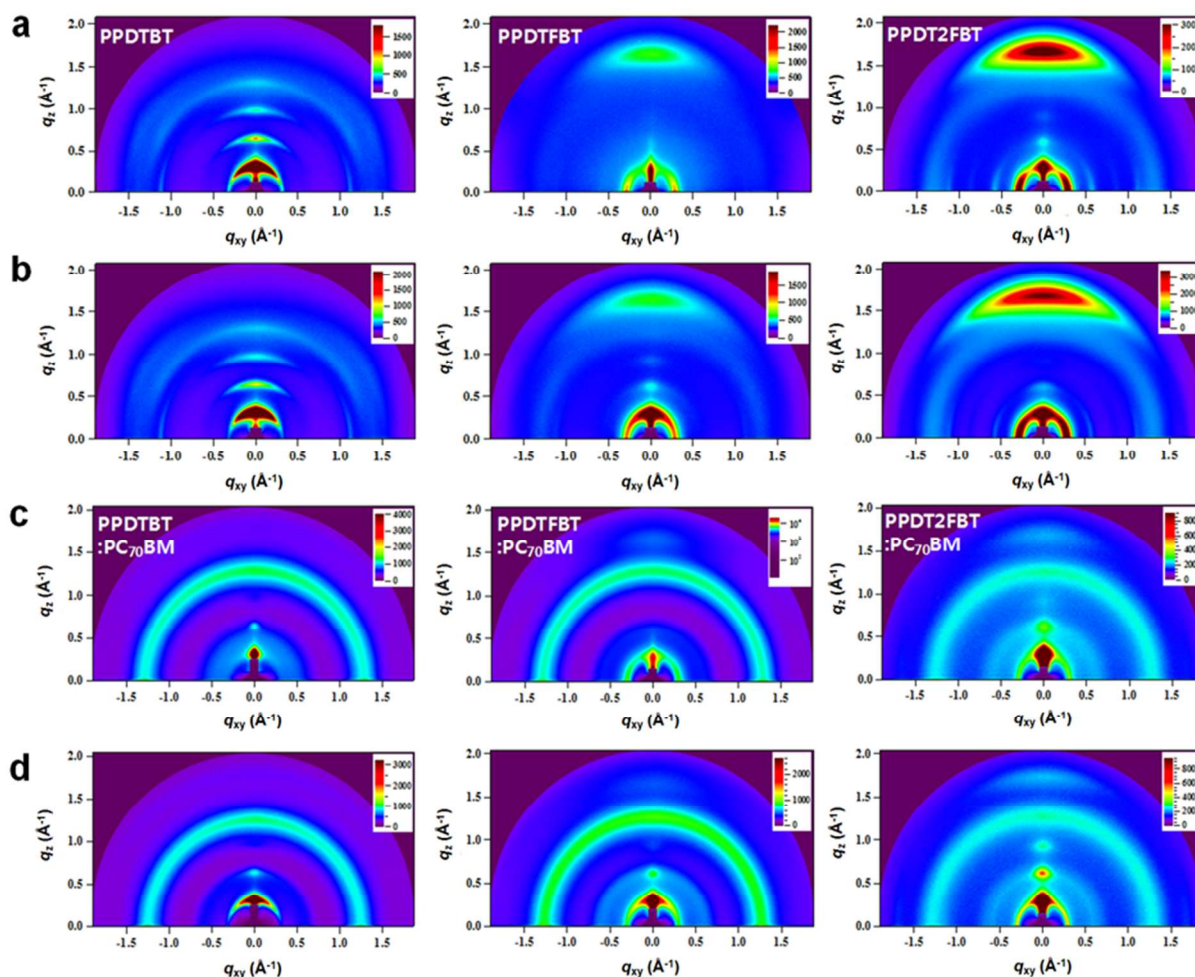


Fig. 9 Grazing incidence wide angle X-ray scattering (GIWAXS) images. GIWAXS images of pristine polymer films (upper two rows) (a) without and (b) with DPE, and polymer:PC₇₀BM blend films (lower two rows) (c) without and (d) with DPE. Left, middle and right panels show the images for PPDTBT, PPDTFBT and PPDT2FBT, respectively.

with tight interchain packing (π - π stacking distance of 3.57–3.59 Å) in the blend films. In addition, we also measured clear molecular weight dependence on the photovoltaic properties. We synthesized more than 20 batches of PPDT2FBT to optimize the photovoltaic characteristics. Among them, the high molecular weight batches (with \sim 40 kDa) showed the PCE over 8-9% but small molecular weight batches showed the relatively lower PCE values (\sim 7%). The detailed study on the molecular weight dependence is now under investigation. Furthermore, this work also demonstrates a high PCE of over 7% (without any post-treatments) with long-term thermal stability at 130 °C for \sim 200 h. These new polymers provide a great possibility to overcome the efficiency barrier of 10% and accelerate the real application of plastic solar cells.

4. EXPERIMENTAL SECTION

4.1. General

A microwave reactor (Biotage InitiatorTM) was used to synthesize the polymers. ¹H and ¹³C NMR spectra were

recorded on a JEOL (JNM-AL300) FT NMR system operating at 300 MHz and 75 MHz, respectively. UV-vis spectra were obtained with a JASCO V-630 spectrophotometer. The number- and weight-average molecular weights of the polymers were determined by gel-permeation chromatography (GPC) with *o*-dichlorobenzene as an eluent at 80 °C on an Agilent GPC 1200 series, relative to polystyrene standards. Cyclic voltammetry (CV) experiments were performed with Versa STAT 3 analyzer. All CV measurements were carried out in 0.1 M tetrabutylammoniumtetrafluoroborate (Bu₄NBF₄) in acetonitrile with a conventional three-electrode configuration employing a platinum wire as a counter electrode, platinum electrode coated with a thin polymer film as a working electrode, and Ag/Ag⁺ electrode as a reference electrode (scan rate: 50 mV·s⁻¹). Thermogravimetric analysis (2050 TGA V5.4A) and differential scanning calorimetry (DSC Q200 V24.4) measurements were performed at a heating and cooling rate of 10 °C·min⁻¹ under nitrogen (purity, 99.999%). The nanoscale morphology of the polymer films was measured using high-resolution transmission electron microscopy (HR-TEM) (JEM-2100, Cs corrector). Atomic force microscopy (AFM) images

(1.5 μm \times 1.5 μm) were obtained using a Veeco AFM microscope in a tapping mode. Carrier mobilities were calculated by the space charge limited current method using hole-only (ITO/PEDOT:PSS/active layer/Au) and electron-only (FTO/active layer/Al, FTO: fluorine-doped tin oxide) diodes by fitting their J - V characteristics with the Mott-Gurney equation (Eq. 1).^{37,38} Corrections were made for the built-in potential (V_0) of the devices due to differences in the work functions of the electrodes and for the loss in potential due to series resistance (V_{RS}) using the equation $V_{RS} = I \times R_S$. The thickness (L) of each device was measured after collecting J - V data using an atomic force microscope and a value of 3 was assumed for ϵ_r .

4.2. Synthesis of polymers.

In a glove box, M1 (0.230 g, 0.32 mmol), M4 (0.263 g, 0.32 mmol), tris(dibenzylideneacetone)dipalladium(0) (4 mol%) and tri(*o*-tolyl)phosphine (8 mol%) and 1 mL chlorobenzene were added in a 5 mL microwave vial. The polymerization reaction mixture was heated at 80 $^\circ\text{C}$ (65 W, 10 min), at 100 $^\circ\text{C}$ (70 W, 10 min) and at 140 $^\circ\text{C}$ (80 W, 40 min) in a microwave reactor. The polymer was end-capped by addition of 2-tributylstannylthiophene (0.05 g, 0.14 mmol) and the mixture was further reacted at 140 $^\circ\text{C}$ for 20 min. The solution was cooled down and 2-bromothiophene (0.09 g, 0.53 mmol) was added by syringe. The reaction solution was heated 140 $^\circ\text{C}$ for another 20 min. After the reaction was finished, the crude PPDTBT polymer was precipitated into the mixture of methanol and HCl (36%) (350 mL:10 mL) and further purified by Soxhlet extraction with acetone, hexane and chloroform. The extracted PPDTBT polymer in chloroform was precipitated into MeOH, filtered and dried under vacuum. PPDTFBT and PPDT2FBT were synthesized by following the same procedure for PPDTBT.

Poly[(2,5-bis(2-hexyldecyloxy)phenylene)-alt-(4,7-di(thiophen-2-yl)benzo[c][1,2,5]-thiadiazole)] (PPDTBT). Yield: 70%. Number-average molecular weight (M_n) = 17.8 kDa, polydispersity index (PDI) = 2.4. δ_H (300 MHz; CDCl_3) 0.86-2.02 (62 H, br), 4.10 (4H, br), 7.48 (2H, br), 7.69 (2H, br), 7.91 (2H, br), 8.19 (2H, br).

Poly[(2,5-bis(2-hexyldecyloxy)phenylene)-alt-(5-fluoro-4,7-di(thiophen-2-yl)benzo[c][1,2,5]-thiadiazole)] (PPDTFBT). Yield: 65%. M_n = 29.8 kDa, PDI = 2.4. δ_H (300 MHz; CDCl_3) 0.86-2.02 (62H, br), 4.06 (4H, br), 7.06-8.20 (7H, br).

Poly[(2,5-bis(2-hexyldecyloxy)phenylene)-alt-(5,6-difluoro-4,7-di(thiophen-2-yl)benzo[c][1,2,5]-thiadiazole)] (PPDT2FBT). Yield: 67%. M_n = 42.6 kDa, PDI = 2.8. δ_H (300 MHz; CDCl_3) 0.86-2.02 (62H, br), 4.00 (4H, br), 7.06-8.20 (6H, br).

4.3. Fabrication and characterization of PSCs.

ITO-coated glass substrates were cleaned by ultrasonication in deionized water, acetone and iso-propanol, and then dried in an oven for 12 h. After UV-ozone treatments for 10 min, PEDOT:PSS solution (Baytron P VPAI 4083, H. C. Starck) was spin-coated onto the ITO substrate at 5000 rpm for 40 s and

then baked at 140 $^\circ\text{C}$ for 10 min. For deposition of the active layer, blend solutions of polymer (1 wt%):PC₇₀BM (1.5 wt%) dissolved in DCB or in CB (with/without 2 vol% diphenyl ether) were spin-cast on top of the PEDOT:PSS layer in a nitrogen-filled glove box. For methanol (MeOH) treatment, MeOH was spin-cast at 1000 rpm for 40 s on top of the active layer. Subsequently, an Al (100 nm) electrode was deposited on top of the active layer under vacuum ($<10^{-6}$ Torr) by thermal evaporation. The area of the Al electrode defines the active area of the device as 13.0 mm². For the characterization of PSCs, their current density-voltage (J - V) characteristics were measured using a Keithley 2635A Source Measure Unit. Solar cell performance was tested with an Air Mass 1.5 Global (AM 1.5 G) solar simulator under an irradiation intensity of 100 mW $\cdot\text{cm}^{-2}$. EQE measurements were obtained using a PV measurement QE system using monochromatic light from a xenon lamp under ambient conditions. The monochromatic light was chopped at 100 Hz and intensity was calibrated relative to a standard Si photodiode using a lock-in-amplifier. A mask (13.0 mm²) made of thin metal was used for J - V characteristics and EQE measurements.

4.4. GIWAXS measurements.

GIWAXS measurements were carried out at PLS-II 9A U-SAXS beam line of Pohang Accelerator Laboratory. X-ray coming from the in-vacuum undulator (IVU) was monochromated ($E_k = 11.24$ keV, $\lambda = 1.103$ \AA) using a Si(111) double crystal monochromator and focused horizontally and vertically at the sample position (450 (H) \times 60 (V) μm^2 in FWHM) using K-B-type focusing mirror system. The GIWAXS sample stage was equipped with a 7-axis motorized stage for the fine alignment of the thin sample and the incidence angle of X-rays was adjusted to 0.12 $^\circ$ -0.14 $^\circ$. GIWAXS patterns were recorded with a 2D CCD detector (Rayonix SX165, USA), and X-ray irradiation time was 0.5-5 s depending on the saturation level of the detector. The diffraction angle was calibrated with a sucrose standard (monoclinic, P21, $a = 10.8631$ \AA , $b = 8.7044$ \AA , $c = 7.7624$ \AA , $\beta = 102.938^\circ$) and the sample-to-detector distance was approximately 232 mm. Samples for GIWAXS measurements were prepared by spin-coating polymer or polymer:PC₇₀BM blend solutions on top of the Si substrates. We also checked GIWAXS data on top of the PEDOT:PSS/Si layer. We obtained same morphologies with and without PEDOT:PSS layer on the Si substrate.

Acknowledgements

T. L. Nguyen, H. Choi and S.-J. Ko contributed equally to this work. This work was supported by the National Research Foundation (NRF) of Korea (2012R1A1A2005855, 2012M3A6A7055540, 2013M3C1A3065522, 2009-0093020) and the International Cooperation of the Korea Institute of Energy Technology Evaluation and Planning (KETEP) grant funded by the Korea government Ministry of Knowledge Economy (2012T100100740).

Notes and references

- ^a Department of Nanofusion Engineering, Department of Cogno-Mechatronics Engineering, Pusan National University, Miryang 627-706, Korea.
- ^b Interdisciplinary School of Green Energy and KIER-UNIST Advanced Center for Energy, Ulsan National Institute of Science and Technology (UNIST), Ulsan 689-798, Korea.
- ^c Pohang Accelerator Laboratory, San 31, Hyoja-dong, Pohang 790-784, Korea.
- † Electronic Supplementary Information (ESI) available: Synthetic details for monomers, DFT calculation, additional GIWAXS and photovoltaic characterization data. See DOI: 10.1039/b000000x/
- G. Li, R. Zhu and Y. Yang, *Nature Photon.*, 2012, **6**, 153-161; S. B. Darling and F. You *RSC Adv.*, 2013, **3**, 17633-17648.
 - L. Huo, S. Zhang, X. Guo, F. Xu, Y. Li and J. Hou, *Angew. Chem. Int. Ed.*, 2011, **50**, 9697-9702.
 - T. Y. Chu, J. Lu, S. Beaupre, Y. Zhang, J. R. Pouliot, S. Wakim, J. Zhou, M. Leclerc, Z. Li, J. Ding and Y. Tao, *J. Am. Chem. Soc.*, 2011, **133**, 4250-4253.
 - L. Dou, J. You, J. Yang, C. C. Chen, Y. He, S. Murase, T. Moriarty, K. Emery, G. Li and Y. Yang, *Nature Photon.*, 2012, **6**, 180-185.
 - J. K. Kim, K. Lee, N. E. Coates, D. Moses, T. Q. Nguyen, M. Dante and A. J. Heeger, *Science.*, 2007, **317**, 222-225.
 - C. Cabanetos, A. E. Labban, J. A. Bartelt, J. D. Douglas, W. R. Mateker, J. M. J. Fréchet, M. D. McGehee and P. M. Beaujuge, *J. Am. Chem. Soc.*, 2013, **135**, 4656-4659.
 - Z. He, C. Zhong, S. Su, M. Xu, H. Wu and Y. Cao, *Nature Photon.*, 2012, **6**, 591-595.
 - H. J. Son, L. Lu, W. Chen, T. Xu, T. Zheng, B. Carsten, J. Strzalka, S. B. Darling, L. X. Chen and L. Yu, *Adv. Mater.*, 2013, **25**, 838-843.
 - H.-C. Chen, Y. H. Chen, C.-C. Liu, Y.-C. Chien, S.-W. Chou and P.-T. Chou, *Chem. Mater.*, 2012, **24**, 4766-4772.
 - B. C. Schroeder, Z. Huang, R. S. Ashraf, J. Smith, P. D'Angelo, S. E. Watkins, T. D. Anthopoulos, J. R. Durrant and I. McCulloch, *Adv. Funct. Mater.*, 2012, **22**, 1663-1670.
 - Y. Zhang, S.-C. Chien, K.-S. Chen, H.-L. Yip, Y. Sun, J. A. Davies, F. C. Chen and A. K.-Y. Jen, *Chem. Commun.*, 2011, **47**, 11026-11028.
 - Z. Li, J. Lu, S.-C. Tse, J. Zhou, X. Du, Y. Tao and J. Ding, *J. Mater. Chem.*, 2011, **21**, 3226-3233.
 - Y. Wang, S. R. Parkin, J. Gierschner and M. D. Watson, *Org. Lett.*, 2008, **10**, 3307-3310.
 - F. Babudri, G. M. Farinola, F. Naso and R. Ragni, *Chem. Commun.*, 2007, 1003-1022.
 - K. Reichenbacher, H. I. Suss and J. Hulliger, *Chem. Soc. Rev.*, 2005, **34**, 22-30.
 - W. Lee, H. Choi, S. Hwang, J. Y. Kim and H. Y. Woo, *Chem. Eur. J.*, 2012, **18**, 2551-2558.
 - X. Guo, J. Quinn, Z. Chen, H. Usta, Y. Zheng, Y. Xia, J. W. Hennek, R. P. Ortiz, T. J. Marks and A. Facchetti, *J. Am. Chem. Soc.*, 2013, **135**, 1986-1996.
 - X. Guo, F. S. Kim, S. A. Jenekhe and M. D. Watson, *J. Am. Chem. Soc.*, 2009, **131**, 7206-7207.
 - D. Beljonne, G. Pourtois, C. Silva, E. Hennebicq, L. M. Herz, R. H. Friend, G. D. Scholes, S. Setayesh, K. Müllen and J. L. Brédas, *Proc. Natl. Acad. Sci. U.S.A.*, 2002, **99**, 10982-10987.
 - J. L. Bredas, G. B. Street, B. Themans and J. M. Andre, *J. Chem. Phys.*, 1985, **83**, 1323-1329.
 - R. A. Street, J. E. Northrup and A. Salleo, *Phys. Rev.*, 2005, **B71**, 165202.
 - L. Biniek, C. L. Chochos, N. Leclerc, O. Boyron, S. Fall, P. Lévêque and T. Heiser, *J. Polym. Sci. Part A: Polym. Chem.*, 2012, **50**, 1861-1868.
 - J.-F. Jheng, Y.-Y. Lai, J.-S. Wu, Y.-H. Chao, C.-L. Wang and C.-S. Hsu, *Adv. Mater.*, 2013, **25**, 2445-2451.
 - J. E. Carlé, J. W. Andreasen, M. Jørgensen and F. C. Krebs, *Sol. Energy Mater. Sol. Cells.*, 2010, **94**, 774-780.
 - W. Lee, G.-H. Kim, S.-J. Ko, S. Yum, S. Hwang, S. Cho, Y.-H. Shin, J. Y. Kim and H. Y. Woo, *Macromolecules*, 2014, **47**, 1604-1612.
 - S. Yum, T. An, X. Wang, W. Lee, M. A. Uddin, Y. J. Kim, T. L. Nguyen, S. Xu, S. Hwang, C. Park and H. Y. Woo, *Chem. Mater.*, 2014, **26**, 2147-2154.
 - S. Yum, T. K. An, X. Wang, M. A. Uddin, T. L. Nguyen, S. Xu, H. Ryu, Y. J. Kim, S. Hwang, C. E. Park, H. Y. Woo, *Pure Appl. Chem.*, 2014, DOI: 10.1515/pac-2014-0205.
 - N. E. Jackson, B. M. Savoie, K. L. Kohlstedt, M. O. D. L. Cruz, G. C. Schatz, L. X. Chen and M. A. Ratner, *J. Am. Chem. Soc.*, 2013, **135**, 10475-10483.
 - Y. Zhao and D. G. Truhlar, *Theor. Chem. Account.*, 2008, **120**, 215-241.
 - Y. Zhao and D. G. Truhlar, *Acc. Chem. Research.*, 2008, **41**, 157-167.
 - M. Doemer, I. Tavernelli and U. Rothlisberger, *J. Chem. Theory Comput.*, 2013, **9**, 955-964.
 - K. B. Bravaya, E. Epifanovsky and A. I. Krylov, *J. Phys. Chem. Lett.*, 2012, **3**, 2726-2732.
 - M. Walker, A. J. A. Harvey, A. Sen and C. E. H. Dessent, *J. Phys. Chem. A*, 2013, **117**, 12590-12600.
 - H.-Y. Chen, J. Hou, A. E. Hayden, H. Yang, K. N. Houk, and Y. Yang, *Adv. Mater.*, 2010, **22**, 371-375.
 - A. C. Stuart, J. R. Tumbleston, H. Zhou, W. Li, S. Liu, H. Ade and W. You, *J. Am. Chem. Soc.*, 2013, **135**, 1806-1815.
 - H. Bronstein, J. M. Frost, A. Hadipour, Y. Kim, C. B. Nielsen, R. S. Ashraf, B. P. Rand, S. Watkins and I. McCulloch, *Chem. Mater.*, 2013, **25**, 277-285.
 - P. Kumar, C. Bilén, K. Feron, X. Zhou, W. J. Belcher and P. C. Dastoor, *App. Phys. Lett.*, 2014, **104**, 193905; G. Griffini, J. D. Douglas, C. Piliago, T. W. Holcombe, S. Turri, J. M. J. Fréchet and J. L. Mynar, *Adv. Mater.*, 2011, **23**, 1660-1664.
 - J. Peet, N. S. Cho, S. K. Lee and G. C. Bazan, *Macromolecules*, 2008, **41**, 8655-8659.
 - C. Piliago, T. W. Holcombe, J. D. Douglas, C. H. Woo, P. M. Beaujuge and J. M. J. Fréchet, *J. Am. Chem. Soc.*, 2010, **132**, 7595-7597.
 - J. Peet, J. Y. Kim, N. E. Coates, W. L. Ma, D. Moses, A. J. Heeger and G. C. Bazan, *Nature Mater.*, 2007, **6**, 497-500; H.-C. Liao, C.-C. Ho, C.-Y. Chang, M.-H. Jao, S. B. Darling and W.-F. Su, *Materials Today*, 2013, **16**, 326-336.
 - L. Chang, H. W. A. Lademann, J.-B. Bonekamp, K. Meerholz and A. J. Moulé, *Adv. Funct. Mater.*, 2011, **21**, 1779-1787.
 - J. H. Seo, A. Gutacker, Y. Sun, H. Wu, F. Huang, Y. Cao, U. Scherf, A. J. Heeger and G. C. Bazan, *J. Am. Chem. Soc.*, 2011, **133**, 8416-8419.

- 43 H. Zhou, Y. Zhang, J. Seifert, S. D. Collins, C. Luo, G. C. Bazan, T.-Q. Nguyen and A. J. Heeger, *Adv. Mater.*, 2013, **25**, 1646-1652.
- 44 H.-Y. Chen, J. Hou, S. Zhang, Y. Liang, G. Yang, Y. Yang, L. Yu, Y. Wu and G. Li, *Nature Photon.*, 2009, **3**, 649-653.
- 45 Y. Liang, Z. Xu, J. Xia, S.-T. Tsai, Y. Wu, G. Li, C. Ray and L. Yu, *Adv. Mater.*, 2010, **22**, E135-E138.
- 46 X. Yang, J. Loos, S. C. Veenstra, W. J. H. Verhees, M. M. Wienk, J. M. Kroon, M. A. J. Michels and R. A. J. Janssen, *Nano Lett.*, 2005, **5**, 579-583.
- 47 A. R. V. Benvenho, R. Lessmann, I. A. Hummelgen, R. M. Q. Mello, R. W. C. Li, F. F. C. Bazito and J. Gruber, *Mater. Chem. Phys.*, 2006, **95**, 176-182.
- 48 Y. Shen, A. R. Hosseini, M. H. Wong and G. G. Malliaras, *Chem. Phys. Chem.*, 2004, **5**, 16-25.
- 49 P. W. M. Blom, M. J. M. de Jong and M. G. van Munster, *Phys. Rev. B*, 1997, **55**, R656-R659.
- 50 L. Ye, S. Zhang, W. Ma, B. Fan, X. Guo, Y. Huang, H. Ade, and J. Hou, *Adv. Mater.*, 2012, **24**, 6335-6341; W. Chen, M. P. Nikiforov and S. B. Darling, *Energy Environ. Sci.*, 2012, **5**, 8045-8074.
- 51 X. Guo, N. Zhou, S. J. Lou, J. Smith, D. B. Tice, J. W. Hennek, R. P. Ortiz, J. T. L. Navarrente, S. Li, J. Strzalka, L. X. Chen, R. P. H. Chang, A. Facchetti and T. J. Marks, *Nature Photon.*, 2013, **7**, 825-833.